Analysis of long range studies in the LHC - comparison with the model

Dobrin Kaltchev, TRIUMF, Vancouver, Canada
Werner Herr, CERN, Geneva, Switzerland

Abstract

We find that the observed dependencies (scaling) of long-range beam-beam effects on the beam separation and intensity are consistent with the simple assumption that, all other parameters being the same, the quantity preserved during different setups is the first order smear as a function of amplitude.

INTRODUCTION

Proposed method

In several Machine Development (MD) studies, see [1] and the references therein, reduced crossing angles have been used to enhance long-range beam-beam effects and thus facilitate their measurement. The basic assumption taken in this paper is that under such conditions a single nonlinearity, the one caused by beam-beam, dominates the dynamics. Hence the method followed: we choose some simple low-order dynamical quantity that characterizes phase space distortion and assume that when this quantity is the same, the behavior of the system is the same. A most obvious candidate is the first-order smear – r.m.s. deviation of the phase-space ellipse from the perfect one. At a fixed amplitude smear is defined as the averaged generalized Courant-Snyder invariant over the angle variable [8].

An analytical expression was previously found [8] for the smear S as a function of amplitude n_σ. Suppose that the parametric dependence of $S(n)$ on several beam-beam related parameters: relativistic γ, number of particles per bunch N_b, crossing angle α and normalized separations $n_{\mathrm{l.r.}}$ is known. According to the assumption above for two machine configurations *a* and *b* one should have:

$$S(n_\sigma; N_b^a, n_{l.r.}^a, \alpha^a, \gamma^a) = S(n_\sigma; N_b^b, n_{l.r.}^b, \alpha^b, \gamma^b). \quad (1)$$

As a particular application of (1), we considered two experiments where the intensities are N_b^a and N_b^b. All other parameter being the same, given α^a, one can compute the expected α^b. Our task will be to show that the result agrees with observations.

Analytical calculation of invariant and smear

Our derivation of $S(n_\sigma)$ is based on the Lie-algebraic method – concatenation of Lie-factor maps, and is valid only to first order in the beam-beam parameter and in one-dimension, either in horizontal or in vertical plane, but for an arbitrary distribution of beam-beam collisions, head-on or long-range, around the ring.

For a ring with *single head-on collision point*, Hamiltonian perturbation analysis of the beam-beam interaction without or with crossing angle has been done by a number of authors, mostly in the resonant case. Nonlinear invariants of motion, both nonresonant and resonant, were analyzed by Dragt [2] with the one-turn map as observed immediately after the kick being

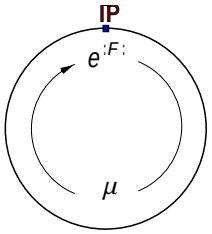

$$R\, e^{:F:} = e^{:h:}. \quad (2)$$

Here $R = e^{:f_2:}$ is the linear one-turn map and the kick-factor F is the beam-beam potential (= - Hamiltonian). For small perturbations and far from resonances, particle coordinates in phase space are restricted on the Poincare surface of section

$$h = const\,. \quad (3)$$

Detailed derivation of h to first order in the beam-beam perturbation strength can be found in A. Chao's lectures:

$$h(J,\phi) = -\mu J + \sum_{n=-\infty}^{\infty} c_n^{(\mathrm{ho})}(J) \frac{n\,\mu}{2\sin\frac{n\mu}{2}} e^{in(\phi+\mu/2)}\,, \quad (4)$$

where μ is the ring phase advance and $c_n^{(\mathrm{ho})}(J)$ are coefficients in the Fourier expansion of F, when the latter is rewritten in action-angle coordinates J, ϕ. The coefficients are shown to be related to the modified Bessel functions. Analytic expressions for the invariant h, first-order smear and second order detuning for the case of nonlinear multipole kicks distributed in an arbitrary way around the ring were derived by Irvin and Bengtsson [4]. Smear, the distortion of the ideal phase-space ellipse, is formally defined in [6]. Finally, notice that extracting the smear is a natural step in the procedure that brings the map into its normal form, [5],

In [7], following the Lie algebraic procedure in [3] and [4] we generalized (4) to describe multiple head-on kicks (IP1 and IP5) for the case of LHC). In [8] an expression was presented valid for arbitrary number of head-on (h.o.) and long-range (l.r.) collisions. This expression, to be derived in detail next, has been used on several occasions to interpret results from Sixtrack simulations.

DERIVATION OF THE INVARIANT

Multiple collision points

The horizontal betatronic motion of a weak-beam test particle depends on its initial amplitude n_σ (in units of σ)

and the collision set: a set of all h. o. and l. r. collisions, a.k.a. interaction points (IPs), that this particle sees over a single revolution. Let us label the set with an index k, limiting ourselves to only IPs located within the main interaction regions IR5 (horizontal crossing) and IR1 (vertical crossing). In case of 50 ns bunch spacing, k ranges from 1 to 34 which includes 32 long-range IPs ($N_{l.r.} = 32$).

The Lie map depends on the above defined collision set through the normalized separations $n_{x,y}^{(k)} = d_{x,y}^{(k)}/\sigma^{(k)}$ and the unperturbed horizontal betatronic phases $\phi^{(k)}$ at the IPs. Here $d_{x,y}$ is the real-space offset of the strong beam centroid in x or y direction and it has been assumed that both the weak- and strong-beam transverse distributions are round Gaussians of the same rms, i.e.:

$$\sigma^{(k)} = \sqrt{\beta^{(k)}\epsilon} \quad (\beta_x^{(k)} = \beta_y^{(k)} \equiv \beta^{(k)}). \tag{5}$$

In (5), $\beta^{(k)}$ are the beta functions and ϵ is the emittance. It will be shown below that off-plane collisions contribute very little to smear, thus after excluding these the problem becomes one-dimensional and may easily be illustrated, Figure 1. Here $n_x^{(k)}$ are the strong-beam centroids in amplitude space: points $(s^{(k)}, n_x^{(k)})$ with s being the distance to IP5 in meters.

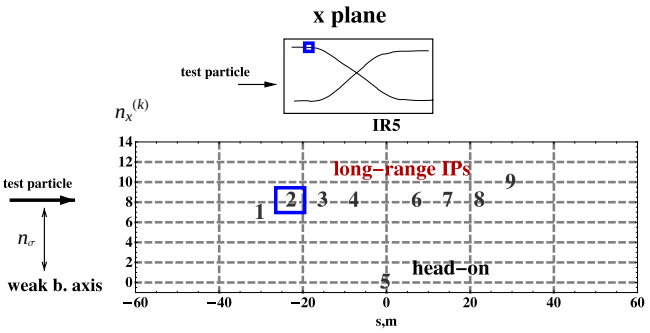

Figure 1: Schematic view of weak and strong beam trajectories in real (top) and amplitude (bottom) spaces. A reduced set is used: $N_{l.r.}$ = 8+8 = 16 (k=1,18).

Beam-beam Hamiltonian

For a single collision, (2), by omitting the superscript k in σ and $n_{x,y}$, the x-motion is described by a kick-factor F (or Hamiltonian H) [8]

$$F = -H(x) = \int_0^P (1 - e^{-\alpha})\frac{d\alpha}{\alpha} = \tag{6}$$

$$= \overline{\gamma} + \Gamma_0(P) + ln(P)\,, \tag{7}$$

$$P = P(x) = \frac{1}{2}\left[(n_x + \frac{x}{\sigma})^2 + n_y^2\right]\,,$$

where F is in units of $\lambda \equiv \frac{N_b r_0}{\gamma}$, r_0 is the classical particle radius, $\Gamma_s(P) \equiv \Gamma(s, P)$ denotes the upper incomplete gamma function [9] and $\overline{\gamma}$ = 0.577216 is the Euler's constant. The corresponding beam-beam kick is:

$$\Delta x' \equiv \frac{d}{dx}F(x) = \frac{\partial F}{\partial P}\frac{dP}{dx} =$$

$$= \frac{2(x+n_x\sigma)}{(x+n_x\sigma)^2+(n_y\sigma)^2}\left[1 - e^{-\frac{(x+n_x\sigma)^2+(n_y\sigma)^2}{2\sigma^2}}\right]. \tag{8}$$

The Fourier expansion of H is:

$$H(n_\sigma, \phi) = \sum_m \mathcal{C}_m e^{im\phi}\,, \tag{9}$$

where $\mathcal{C}_m \equiv \frac{1}{2\pi}\int_0^{2\pi} e^{-im\phi} H\; d\phi$. These coefficients are easily computed numerically by using the implementation of Γ in *Mathematica*, [8]. Further, analytic expressions in the form of single integrals over Bessel functions have been derived in [11]. We display these again in the simplified case $n_y = 0$ (no off-plane collisions):

$$\mathcal{C}_m|_{n_y=0} = \int_0^1 \frac{dt}{t} \times$$

$$\begin{cases} [1 - e^{-\frac{t}{2}n_x^2}e^{-\frac{t}{4}n_\sigma^2}\sum_{k=-\infty}^{\infty} I_{-2k}(t\,n_\sigma n_x)I_k(-\frac{t}{4}n_\sigma^2)] \\ \text{if } m = 0 \quad \text{and} \\ -e^{-\frac{t}{2}n_x^2}e^{-\frac{t}{4}n_\sigma^2}\sum_{k=-\infty}^{\infty} i^m I_{m-2k}(t\,n_\sigma n_x)I_k(-\frac{t}{4}n_\sigma^2) \\ \text{if } m \neq 0. \end{cases}$$

In the head-on case ($n_x^{(k)} = n_y^{(k)} = 0$) the coefficients $\mathcal{C}_m$ reduce to the $c_m^{(\mathrm{ho})}$ from [3]. Notice that in the most interesting case: amplitudes near the dynamic aperture, both n_σ and n_x and hence the Bessel function arguments are large ($\gg 1$).

Our first step is to remove the linear and quadratic parts $F_{(1)} = \frac{\partial F}{\partial x}\big|_{x=0} x$ and $F_{(2)} = \frac{1}{2}\frac{\partial^2 F}{\partial x^2}\Big|_{x=0} x^2$. The nonlinear kick-factor and corresponding kick are:

$$F_{\mathrm{nonl}} = F - F_{(1)} - F_{(2)}\,, \tag{10}$$

$$\Delta x'_{\mathrm{nonl}} \equiv \frac{d}{dx}F_{\mathrm{nonl}}(x)\,.$$

As a next step, we rewrite (10) in action-angle coordinates J, ϕ by substituting in it $x = \sqrt{2J\beta}\sin\phi = n_\sigma\sigma\sin\phi$, where $n_\sigma = \sqrt{2I} = \sqrt{2J/\epsilon}$ is the test particle amplitude (see Eq. A.1 in Appendix). Next, we expand in Fourier series:

$$F_{\mathrm{nonl}}(n_\sigma\,\sigma\,\sin\phi) = c_0 + \sum_{m\neq 0} c_m e^{im\phi}\,. \tag{11}$$

The coefficients c_m are naturally the same as $\mathcal{C}_m$ above, with the exception of c_1 and c_2 which contain additional sin and sin^2 terms, see Eq. A.1.

Lie map and invariant

For an arbitrary set of collisions $n_x^{(k)}$, $\phi^{(k)}$ ($k = 1, N$) we represent the LHC lattice by a combination of linear

elements and nonlinear kicks. It is shown in the Appendix that, to first order in λ, the Lie map has the same form as the one for a single kick (2), where however the factor F is given by the sum:

$$F \equiv \sum_{k=1}^{N} F_{\rm nonl}^{(k)}(n_\sigma, \phi)$$

and $F_{\rm nonl}^{(k)}$ are such that, compared to (11), the kth IP participates with a phase shifted by $\phi^{(k)}$.

$$F_{\rm nonl}^{(k)}(n_\sigma, \phi) \equiv F_{\rm nonl}^{(k)}(x)\Big|_{x \to n_\sigma \sigma^{(k)} sin(\phi+\phi^{(k)})} = \\ = \sum_{m\neq 0} C_m^{(k)} e^{im\phi}\,. \qquad (12)$$

The shift in phase means that the coefficients in (12) are simply related to $c_m^{(k)}$: $C_m^{(k)} \equiv c_m^{(k)} e^{im\phi^{(k)}}$ and still satisfy $C_{-m} = C_m^\star$. Another important property of the expansion is that only the oscillating part is taken (the m=0 term is excluded). The invariant for multiple collision points is (Appendix):

$$h(I,\phi) = -\mu J - \lambda \sum_{k=1}^{N}\sum_{m=1}^{\infty} \frac{m\,\mu\, c_m^{(k)}(I)}{2\sin\left(\frac{m\mu}{2}\right)} e^{im(\phi+\mu/2+\phi^{(k)})} \\ + c.c.$$

The surface of section in phase space is given by $h(I,\phi) = const$. A natural initial condition is now imposed: that the initial point in phase space for a particle starting at $x_0 = n_\sigma\sigma$, i.e. with an amplitude $I_0 \equiv J_0/\epsilon = n_\sigma^2/2$, lies on the curve representing the invariant:

$$h(I,\phi) = h(I_0, \pi/2), \qquad (13)$$

For a fixed I_0, this equation defines implicitly I as a function of ϕ. It satisfies the initial condition $I(0) = I_0$:

$$I(\phi) = I_0 + \sum_{k=1}^{N}\left(dI^{(k)}(\phi) - dI^{(k)}(0)\right)\,,$$

$$dI^{(k)}(\phi) = \qquad (14)$$
$$= \frac{\lambda}{\epsilon}\sum_{m=1}^{M}\left(\frac{m\,c_m^{(k)}(I_0)}{2\sin(m\mu/2)} e^{im(\mu/2+\phi-\phi^{(k)}+\pi/2)} + c.c.\right)$$

Notice that, to first order, the argument in $c_m^{(k)}$ has been replaced with I_0. We have also separated the two sums so that $dI^{(k)}(\phi) - dI^{(k)}(0)$ is the individual contribution of the kth IP. In the same way, a different initial condition may be used (more suitable for plots): $I(0) = I_0$, instead of $I(\pi/2) = I_0$.

The smear $S(n_\sigma)$ is now defined as the normalized r.m.s. of the invariant, i.e. $\sqrt{V}$ with V being the variance:

$$S(n_\sigma) = \sqrt{V}/\langle I\rangle\,,$$
$$V = \tfrac{1}{2\pi}\int (I - \langle I\rangle)^2 d\phi\,, \quad \langle I\rangle = \tfrac{1}{2\pi}\int I d\phi\,.$$

VERIFICATION WITH TRACKING

As an example application, this section studies the very simple collision set that still posses all the symmetries with l.r. set at 8 sigma as depicted on Figure 2. Both IR5 and IR1 are included. The goal here is to test the invariant $I(\phi)$ by tracking with a simple model built with kicks $\Delta x'_{\rm nonl}$ alternating with linear matrices and Sixtrack. The parameters are: energy 3.5 TeV, $N_{\rm b} = 1.2\,10^{11}$ and normalized emittance $\epsilon_n = 2.5\,10^{-6}$. Tracking single particles at various amplitudes with the simple model produces the results shown on Figure 3. A particle starts with $n_\sigma = 3$, or 7 ($I_0 = 4.5$, or 24.5). The c_m are computed with accuracy 10^{-7} – the value of M in (15) as about 40. Since the beam-beam potential changes the linear optics, we need to find the linearly-perturbed matched β-function value at the initial point for tracking. For the plots on Figure 3 this is done in a separate run using a linear kick $(\Delta x')_{\rm lin}$ (only term $\sim x^2$ in the Hamiltonian). This is similar to what is done in Sixtrack. The resultant matched β is used to define the initial coordinate x_0 (through n_σ). The values of the smear are shown on the top of each plot.

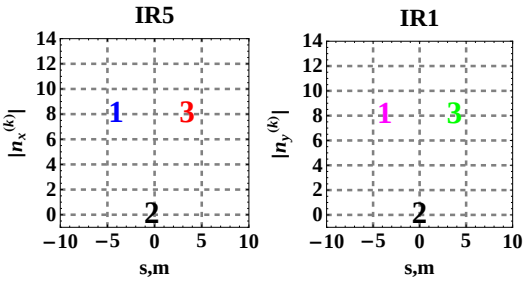

Figure 2: Sample setup: three collisions in each IR5 and IR1. The l.r. are set at 8 sigma.

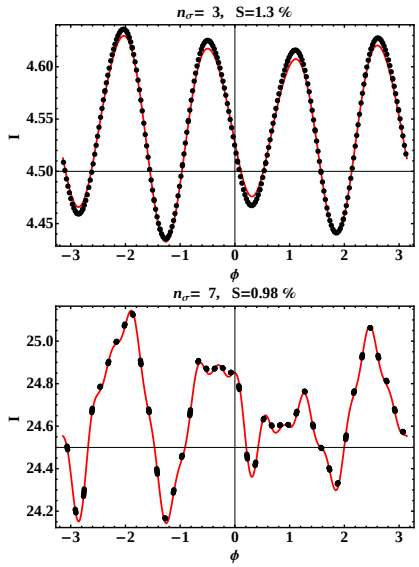

Figure 3: Invariant tested on a simple kick-matrix model. Black points: turn-by-turn coordinates (ϕ, I) for 10^3 turns. Red: invariant $I(\phi)$ (initials chosen so that $I(\pi/2) = I_0$).

Plotting the smear over a range of amplitudes with all three methods: model, Sixtrack and analytic $S(n_\sigma)$ results in Figure 4. Notice that here the images of the strong-beam centroids (see Fig. 1) are represented with vertical gray lines drawn at 0 and 8 sigma. Let us now look at

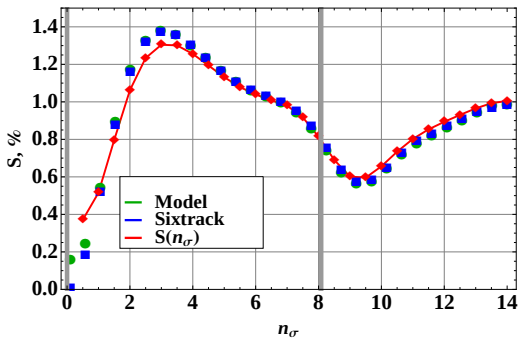

Figure 4: Agreement with Sixtrack.

the individual contributions to $I(\phi)$ of the six IPs at three amplitudes chosen arbitrarily, say $n_\sigma = 1, 3$ and 7. The ex-

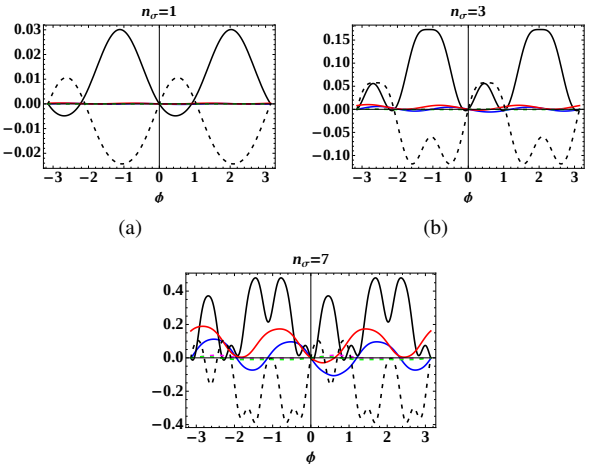

(a) (b) (c)

Figure 5: Individual contributions $dI^{(k)}(\phi) - dI^{(k)}(0)$ – color code as on Fig. 2

cursions (w.r.t. I_0) of the individual invariant surfaces are shown on Fig. 5. Here $I(0) = I_0$. The color code is as on Fig. 2 and in addition for the head-ons we use solid black for IP5 and dashed for IP1. Near the axis ($n_\sigma = 1$), only the two head-ons contribute and, being of opposite signs, nearly compensate each other. At $n_\sigma = 3$, one begins to see long range contributions that grow when $n_\sigma = 7$. At such large amplitudes, the compensation is no longer true. Magenta and green are barely seen, meaning that contribution of off-plane collisions is negligible. Thus in case of test particle moving in the horizontal motion, the contribution of all l.r. in IR1 can be neglected, and vice versa for vertical motion and IP5.

BEHAVIOR OF THE SMEAR $S(n_\sigma)$ NEAR THE DYNAMIC APERTURE

Above some critical strength of beam-beam interaction, i.e. quantities $N_{l.\,r.}$ and/or N_b and/or inverse crossing angle, the first-order theory is no longer an adequate description of the smear. However, as we will see, the behavior of $S(n_\sigma)$ still may be used as an indication for dynamic aperture since it exhibits a local maximum near it. What

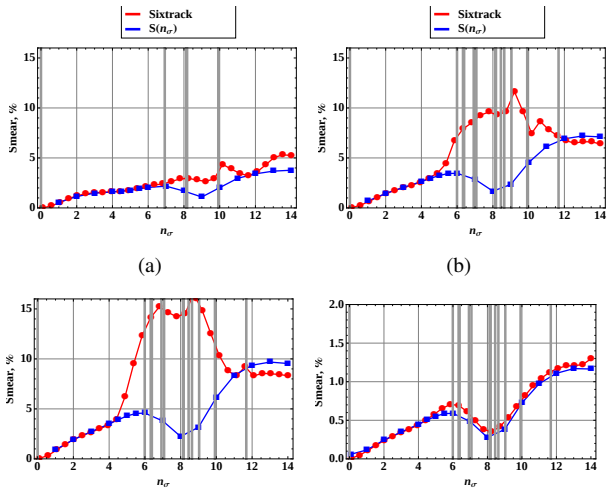

(a) (b) (c) (d)

Figure 6: Various combinations of number of long-range collisions and and bunch intensity to illustrate linear and nonlinear behavior:

	$N_{l.\,r.}$	N_b
a)	16	$1.2\ 10^{11}$;
b)	32	$1.2\ 10^{11}$;
c)	32	$1.6\ 10^{11}$;
d)	32	$0.2\ 10^{11}$.

happens is that the linear behavior, i.e. agreement between the first-order S and Sixtrack at all amplitudes seen on Figure 4 is replaced by what is shown on Figures 6 a), b) and c). The blue ($S(n_\sigma)$) and the red (Sixtrack) curves depart from each other once n_σ approaches amplitudes near the strong beam core, represented by the cluster of vertical gray lines. At this point the exact smear (red) exhibits a steep growth, thus the dynamic aperture is likely to be close to this point while S goes through a maximum and then through a minimum, thus forming a dip. Upon exiting the core, past the last gray line, the red and blue curves nearly remerge. It can be shown that the above property of $S(n_\sigma)$ is a consequence of the left-right symmetry of IR5 and IR1. Namely, the individual contributions (such as red and blue curves on Fig. 2) change sign or flip about the axis each time n_σ crosses a gray line. At this amplitude $S(n_\sigma)$ stops growing and goes through a maximum.

ANALYSIS OF LONG RANGE EXPERIMENTS

Dependence on intensity and crossing angle

We set the parameters as at the MD: energy 3.5 TeV, $\epsilon_n = 2.5\,10^{-6}$ [1], $\beta^\star = 0.6$ m.

Of all collisions sets used at the MD, let us consider three $N_{l.r.}$ =32, 24 and 16. For each of them, two parameters: bunch intensity N_b and (half) crossing angle α uniquely define the dependence the first-order smear on amplitude $S(n_\sigma; N_\mathrm{b}, \alpha)$ through the following procedure. First, being a first-order quantity in λ, the smear is obviously proportional to the intensity: $S \sim N_\mathrm{b}$. Secondly, the dependence of $n^{(k)}_{x,y}$ on the (half) crossing angle α is given by the well known scaling law: $n^{(k)}_{x,y} \sim \alpha\sqrt{\beta^\star}$, where $n^{(k)}_{x,y}$ are taken from some sample lattice built for $\beta^\star = 0.55$ m and $\alpha = 125$. Finally, the phases $\phi^{(k)}$ are assumed to be independent on α.

The dependence on angle is presented on Figure 7. Each blue branch corresponds to $S(n_\sigma; 1.2\times10^{11}, \alpha)$ taken over an amplitude range where it is monotonically increasing hence, as we already know, it will remain in agreement with tracking for any strength of the beam-beam interaction.

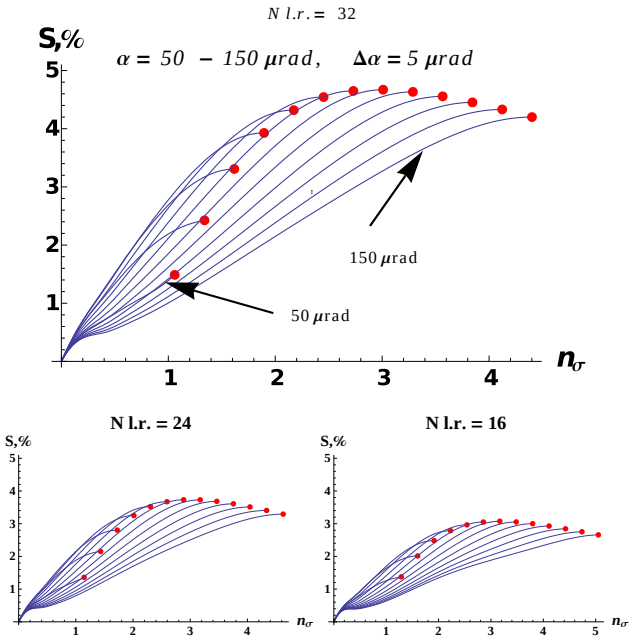

Figure 7: Dependence of the smear(amplitude) graph on the parameter α for $N_{l.r.}$ =32 (top) and $N_{l.r.}$ = 24, 16 (bottom). Each graph is restricted within a domain extending up to its first maximum (red dot) (entrance into the strong-beam core).

Coming now to the MD, the observed losses during reduction of the crossing angle in IP1 are shown on Figures 9 and 10 [1].

[1] Using as an alternative $\epsilon_n = 2\,10^{-6}$ does not change any results.

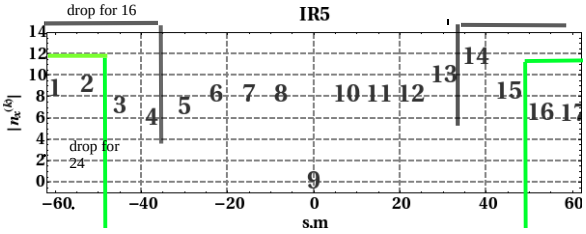

Figure 8: The collision sets for $N_{l.r.}$ =24 and 16 are built by dropping the first and last 2 or 4 elements from the full set ($N_{l.r.}$ =32).

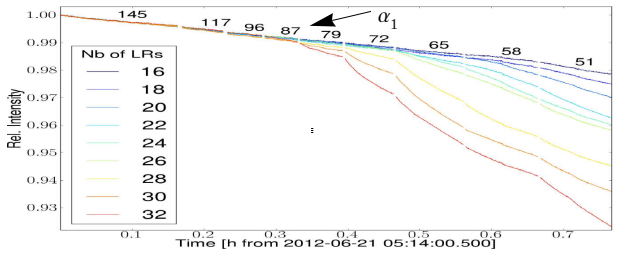

Figure 9: Experiment with $N_\mathrm{b} = 1.2\,10^{11}$: losses start at $\alpha_1 \approx 87$ μrad

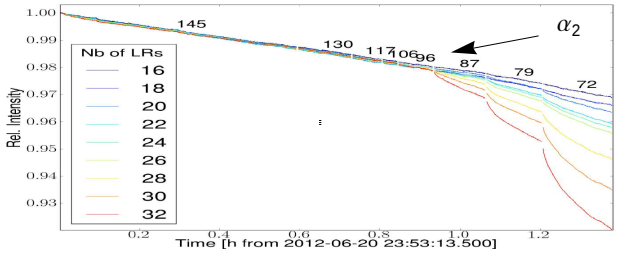

Figure 10: Experiment with $N_\mathrm{b} = 1.6\,10^{11}$: losses start at $\alpha_1 \approx 96$ μrad

Explanation of the case $N_{l.r.}$ =32 (brown curves)

For $N_{l.r.}$ =32 (the full 50-ns collision set shown on Figure 8) we need to explain the brown curves on Fig 9 and 10. Here losses are seen to start at $\alpha_1 \approx 87$ and $\alpha_2 \approx 96$ μrad respectively.

In view of our previous findings, the off-plane losses (in IR5) are neglected and by using the postulate made in the Introduction, Eqn 1, we have:

$$S(n_\sigma; 1.2\,10^{11}, \alpha_1) = S(n_\sigma; 1.6\,10^{11}, \alpha_2), \qquad (15)$$

which is to be solved for the angles.

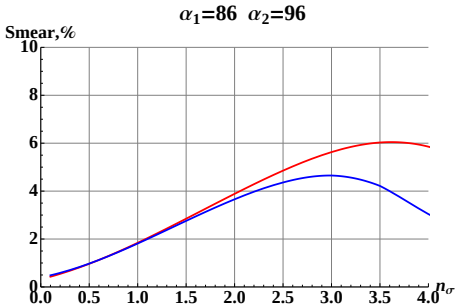

Figure 11: Graphs of $S(n_\sigma; 1.2\,10^{11}, 86)$ (red) and $S(n_\sigma; 1.6\,10^{11}, 96)$ (blue). The smear is seen to be $\approx 3\%$ at 1.5 σ.

Fig 11 demonstrates that a good solution to (15) are angle values $\alpha_1 = 86$, $\alpha_2 = 96$ μrad. Indeed, this Figure shows that (15) is fulfilled not in a single point, but for all amplitudes up to 1.5 σ where the smear reaches about $\approx 3\%$. What has happened of course is that scaling by a factor $1.6/1.2$, but reducing the angle from α_2 to α_1 has nearly exactly preserved one particular blue branch from Figure 7. Conversely, small variations about this solution, say ± 5 μrad, lead to red and blue curves deviatiing from each other as this is seen on Figure 12.

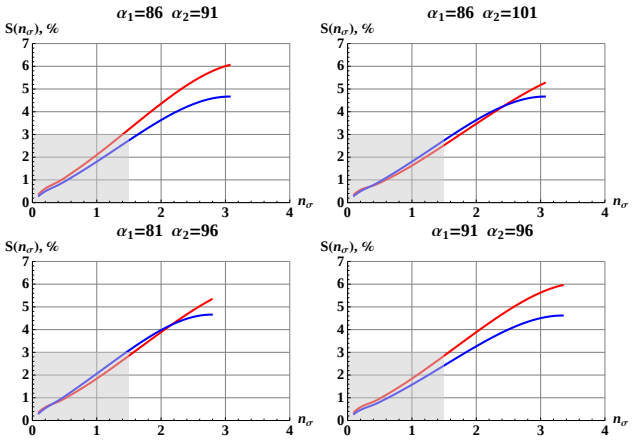

Figure 12: Small variations about the solution ± 5 μrad

Explanation of cases $N_{l.r.}$ =24 and 16 (green and black)

For $N_{l.r.}$ =24 and 16 (reduced collision sets on Figure 8) one needs to explain the green and black decay curves on Fig 9 and 10. By looking now at the bottom two plots in Figure 7, we seek for blue branches that pass through the same maximum-smear point as found above: 3% at 1.5 σ. The resultant branches are plotted on Figures 13 and 14 with solution angles summarized in Table 1. Again, at least a qualitative agreement is observed to the extent allowed by the resolution of Fig 9 and 10.

N_b	green	black
$1.2\,10^{11}$	65	53
$1.6\,10^{11}$	83	72

Table 1: Solutions for the crossing angle in case of green and black decay curves – Figures 9 and 10.

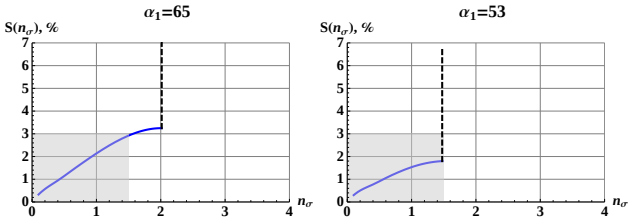

Figure 13: $N_b = 1.2\,10^{11}$

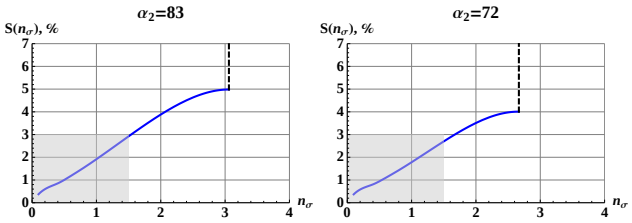

Figure 14: $N_b = 1.6\,10^{11}$

Note that, for the four plots in Figures 13 and 14, on three occasions the 3%-smear line intersects a monotonic part of $S(n_\sigma)$ where, as we already know from Sect. 4, there is an agreement with Sixtrack. The location of the maxium of S (dashed vertical line) is thereby not used to determine the angle. For the remaining case, α=53, the location of the maximum has been used as an indicator of dynamic aperture.

REFERENCES

[1] R. Assmann et al *Results of long-range beam-beam studies - scaling with beam separation and intensity*, CERN-ATS-Note-2012-070 MD

[2] Alex J. Dragt, Oleg G. Jakubowicz, *Analysis of the Beam-Beam Interaction Using Transfer maps*, Proceedings of the Beam Beam Interaction Seminar, Stanford Ca, May 22-23, 1980, SLAC-R-541

[3] A. Chao, Lie Algebra Techniques for Nonlinear Dynamics, `http:www.slac.stanford.edu/~achao`

[4] J. Bengtsson and J. Irwin, *Analytical Calculation of Smear and Tune Shift*, SSC-232, February 1990

[5] E. Forest, Analytical Computation of the Smear, SSC-95.

[6] M. A. Furman and S. G. Peggs, A Standard for the Smear, SSC-N-634.

[7] D. Kaltchev, On beam-beam resonances observed in LHC tracking, TRI-DN-07-9.

[8] W. Herr and D. Kaltchev, Analytical calculation of the smear for long range beam-beam interactions, Proceedings, PAC 2009.

[9] Abramowitz-Stegun, Handbook of Mathematical Functions

[10] W. Herr, D. Kaltchev, Effect of phase advance between interaction points in the LHC on the beam-beam interactions, LHC Project Report 1082, Apr 1 2008

[11] Hamiltonian for Long-range Beam-Beam, Fourier coefficients, TRIUMF Note, Nov 2012.

[12] F. Schmidt, SixTrack, V.4.2 Single Particle Tracking Code Treating Transverse Motion with Synchrotron Oscillations in a Symplectic Manner, CERN/SL/94-56, Jul 2008.

APPENDIX

The nonlinear kick-factor (10) is

$$F_{\rm nonl}(n_\sigma,\phi)=\gamma+\Gamma_0(P)+ln(P)-F_{(1)}-F_{(2)}\,,$$
$$P=\tfrac{1}{2}\left((n_x+n_\sigma\sin\phi)^2+n_y^2\right)\,,$$
$$F_{(1)}=\tfrac{2n_x}{(n_x^2+n_y^2)}\left(1-e^{-\frac{n_x^2+n_y^2}{2}}\right)n_\sigma\sin\phi\,,$$
$$F_{(2)}=\tfrac{-n_x^2+n_y^2+e^{-\frac{n_x^2}{2}-\frac{n_y^2}{2}}\left(n_x^2+n_x^4-n_y^2+n_x^2n_y^2\right)}{\left(n_x^2+n_y^2\right)^2}\times$$
$$\times\, n_\sigma^2\sin^2\phi \qquad\qquad (A.1)$$

By following [4], the Lie map is given by an expression of the form:

$$M_{N+1}e^{:f^{(N)}:}M_N\ldots e^{:f^{(2)}:}M_2e^{:f^{(1)}:}M_1\,,$$
$$f^{(k)}(x)\equiv F^{(k)}_{\rm nonl}(x).$$

Here M_k, are linear operators and for brevity we have replaced $F^{(k)}_{\rm nonl}(x)$ with $f^{(k)}(x)$. We will show that since $F_{\rm nonl}$ depends only on the normalized coordinate x/σ, once we rewrite it in terms of the eigen-coordinates at the kth kick, the local beta-functions $\beta^{(k)}$ disappear while the phase $\phi^{(k)}$ is simply added to ϕ.

By reversing the order, the map transforming the test particle (x,p_x) for one turn around the ring is

$$\mathcal{M}=M_1e^{:f^{(1)}:}M_2e^{:f^{(2)}:}\ldots M_Ne^{:f^{(N)}:}M_{N+1}=$$
$$=e^{:\overline{M}_1f^{(1)}:}e^{:\overline{M}_2f^{(2)}:}\ldots e^{:\overline{M}_Nf^{(N)}:}\overline{M}_{N+1}$$

Reversal of the order means that in the first line all $f^{(k)}$ are now functions of the same initial variables (x,p_x). In the second line, accumulated linear maps $\overline{M}_k=M_1M_2...M_k$ have been applied to transform the initial vector to the kick location. Thus, as a first step, we have moved all kicks to the front of the lattice and $\overline{M}_{N+1}$ is the total one-turn linear Lie operator.

Let us denote matrices corresponding to Lie operators with hats, e.g. $\widehat{M}_{N+1}$. As a second step, with β, α being matched Twiss parameters at the end of the lattice, one uses an A_0 transform that transforms the ring matrix to a rotation (inserting identities $\mathcal{A}_0\mathcal{A}_0^{-1}$ in between the exponents):

$$\widehat{M}_{N+1}\xrightarrow{\widehat{\mathcal{A}}_0}\widehat{R}=\begin{pmatrix}\cos\mu & \sin\mu\\ -\sin\mu & \cos\mu\end{pmatrix},$$

$$\widehat{\mathcal{A}}_0=\begin{pmatrix}\sqrt{\beta} & 0\\ -\alpha/\sqrt{\beta} & 1/\sqrt{\beta}\end{pmatrix}.$$

The two steps above combined are equivalent to replacing the argument of f by $\widetilde{x}_k$ – the eigen-coordinate at the kth location. To see this, apply the $\mathcal{A}_0$ transform to both kick-factor and coordinate:

$$\mathcal{A}_0\overline{M}_kf^{(k)}(x)=f^{(k)}(\mathcal{A}_0\overline{M}_kx)=f^{(k)}(\widetilde{x}_k)\,,$$

$$\widetilde{x}_k\equiv\mathcal{A}_0\overline{M}_kx=\sqrt{2\beta^{(k)}J}\sin\left(\phi+\phi^{(k)}\right)\,.$$

One can now drop the $\mathcal{A}_0$ on both sides of $\mathcal{M}$ and consider the map:

$$\mathcal{M}=e^{:\widetilde{f}^{(1)}:}e^{:\widetilde{f}^{(2)}:}\ldots e^{:\widetilde{f}^{(N)}:}R$$
$$\widetilde{f}^{(k)}(J,\phi)=f^{(k)}(\widetilde{x}_k)$$
$$R=e^{:f_2:},\qquad :f_2:=-\mu J.$$

To first order, one can just sum the Lie-factors:

$$\mathcal{M}\approx e^{:F:}\,R=e^{:h:},\qquad F\equiv\textstyle\sum_{k=1}^N\widetilde{f}^{(k)}.$$

By noticing that above, as in [4], R precedes the kick, while in (2) and [3] the kick is assumed to be at the end of the lattice, our map is identical to (2).

The first order invariant h is now found with the BCH theorem. Let us write $F=\bar{F}+F^\star$ where $F^\star$ is the oscillating part. By taking only $F^\star$:

$$h(J,\phi)=f_2+\frac{:f_2:}{1-e^{-:f_2:}}F^\star \quad (A.2)$$
$$F^\star\equiv\sum_{k=1}^N(\widetilde{f}^{(k)})^\star$$

where according to (12)

$$(\widetilde{f}^{(k)})^\star=\sum_{m\neq0}C_m^{(k)}e^{im\phi}=\sum_{m=1}^\infty\left(C_m^{(k)}e^{im\phi}+cc\right)\,.$$

A basic property of $:f_2:$ is to operate in a simple way on functions of J, or eigen-vectors $e^{in\phi}$. Also functions $G(f_2)$ can easily be applied to eigen-vectors:

$$:f_2:e^{in\phi}=i\,n\,\mu\,e^{in\phi}.$$

$$G(:f_2:)e^{in\phi}=G(i\,n\,\mu)e^{in\phi}.$$

If we choose $G(:f_2:)\equiv\frac{:f_2:}{1-e^{:f_2:}}$, then we have:

$$:G(f_2):e^{im\phi}=$$
$$=G(im\mu)e^{im\phi}=$$
$$=\frac{im\mu}{1-e^{-im\mu}}e^{im\phi}=$$
$$=\frac{i\,m\,\mu\,e^{im\phi}}{e^{i\,m\,\mu/2}-e^{-i\,m\,\mu/2}}e^{i\,m\,\mu/2}=$$
$$=\frac{m\,\mu\,e^{im\phi}}{2\,\sin\left(m\,\mu/2\right)}e^{i\,m\,\mu/2}.$$

By substituting all these in (A.2) and using the property $C_m^{(k)} = c_m^{(k)} e^{im\phi^{(k)}}$ we get:

$$\begin{aligned} & h(J,\phi) = \\ = \quad & -\mu J - \lambda \sum_{k=1}^{N} \sum_{m=1}^{\infty} \left(\frac{m\ \mu\ c_m^{(k)}}{2\sin\left(m\mu/2\right)} e^{im(\mu/2+\phi+\phi^{(k)})} + c.c. \right) \end{aligned}$$